Green Chemistry

Temperature-dependent phase behaviour of tetrahydrofuran-water alters solubilization of xylan to improve co-production of furfurals from lignocellulosic biomass

Temperature-dependent phase behaviour of tetrahydrofuran-water alters solubilization of xylan to improve co-production of furfurals from lignocellulosic biomass

Micholas Dean Smith[a,b], Charles M. Cai[c,d], Xiaolin Cheng[a], Loukas Petridis[a, b], and Jeremy C. Smith[a,b]*

[a] Center for Molecular Biophysics, University of Tennessee/Oak Ridge National Laboratory, Oak Ridge, TN, 37830 USA

[b] Department of Biochemistry and Cellular and Molecular Biology, University of Tennessee, M407 Walters Life Sciences, 1414 Cumberland Avenue, Knoxville, TN 37996

[c] Center for Environmental Research and Technology (CE-CERT), Bourns College of Engineering, University of California, Riverside, 1084 Columbia Avenue, Riverside USA

[d] Department of Chemical and Environmental Engineering, Bourns College of Engineering, University of California, Riverside, 446 Winston Chung Hall, 900 University Ave., Riverside, USA

KEYWORDS: Xylose, Xylan, Hemicellulose, CELF, THF, Co-solvent, Pretreatment, Biomass

ABSTRACT: Xylan is an important polysaccharide found in the hemicellulose fraction of lignocellulosic biomass that can be hydrolysed to xylose and further dehydrated to the furfural, an important renewable platform fuel precursor. Here, pairing molecular simulation and experimental evidences, we reveal how the unique temperature-dependent phase behaviour of water-tetrahydrofuran (THF) co-solvent can delay xylan solubilization to synergistically improve catalytic co-processing of biomass to furfural and 5-HMF. Our results indicate, based on polymer correlations between polymer conformational behaviour and solvent quality, that both co-solvent and aqueous environments serve as 'good' solvents for xylan. Interestingly, the simulations also revealed that unlike other cell-wall components (*i.e.,* lignin and cellulose), the make-up of the solvation shell of xylan in THF-water is dependent on the temperature-phase behaviour. At temperatures between 333K and 418K, THF and water become immiscible, and THF is evacuated from the solvation shell of xylan, while above and below this temperature range, THF and water are both present in the polysaccharide's solvation shell. This suggested that the solubilization of xylan in THF-water may be similar to aqueous-only solutions at temperatures between 333K and 418K and different outside this range. Experimental reactions on beachwood xylan corroborate this hypothesis by demonstrating 2-fold reduction of xylan solubilization in THF-water within a miscible temperature regime (445K) and unchanged solubilization within an immiscible regime (400K). Translating this phase-dependent behaviour to processing of maple wood chips, we demonstrate how the weaker xylan solvation in THF-water under miscible conditions can delay furfural production from xylose, allowing 5-HMF production from cellulose to "catch-up" such that their high yield production from biomass can be synergized in a single pot reaction.

Introduction:

Understanding solvent interactions with biomass polysaccharides is crucial for determining molecular principles to guide the design of effective chemical processes to deconstruct and convert recalcitrant biomass to sugars, renewable liquid fuels, and commodity chemicals[1-3]. Recently, the Co-solvent Enhanced Lignocellulosic Fractionation (CELF) pretreatment method has been shown to greatly enhance the deconstruction and conversion of lignocellulose[4-6]. CELF pretreatment makes use of mixtures of tetrahydrofuran (THF), water, and dilute acid at temperatures near 445K to fractionate lignocellulosic biomass[4-6]. Further, depending on process conditions, the pretreatment can be "tuned" to achieve high yields of either fermentable sugars[4] (for biological processing) or renewable platform chemicals[5, 6]. The underlying mechanism for the high performance and "tunability" (sugar vs. platform chemical production) granted by this co-solvent pretreatment system is poorly understood, and thus an examination into the interactions of THF, water, and biomass during CELF pretreatment is necessary.

The defining feature of CELF pretreatment, as noted above, is the use of THF-water co-solvents. THF-water co-solvent systems themselves are quite interesting as they exhibit an unusual high temperature closed-loop miscibility gap[7-15]. The miscibility gap, where below a critical temperature and above a second critical temperature the solvents are mixed while between these temperatures the two solvents spontaneously demix, is located between 333K and 418K for 1:1 THF-water volume ratios, just below the CELF pretreatment temperatures of 445K-475K. Although not used in CELF, the gap is particularly interesting as it may permit processing strategies that involve both biphasic and monophasic solvent regimes.

Plant cell walls are composed primarily, of polysaccharides (cellulose and hemicellulose) and amorphous (polyphenolic) lignin[16, 17]. The general structure of lignocellulose is such that cellulose fibres function as the backbone of the cell-wall with hemicellulose and lignin forming a matrix that protects cellulose from both biotic and abiotic stress[16, 17]. In recent work, we have paired computational and experimental results to explore the behaviour of cellulose and lignin under THF-water co-solvent conditions[18-21].

Across a wide temperature range encompassing both the miscible and immiscible THF-water phases, lignin polymers were found to be preferentially solvated by THF along with a small fraction of water trapped near lignin monomer-monomer α- or β-O-4 ether linkages[18, 20]. Lignin polymers were also found to adopt random-coil conformations, much like those of linear polymers under θ-solvent conditions, at temperatures ranging from 303K to 445K, including temperatures within the THF-water biphasic (miscibility gap) regime.

Cellulose fibres, like lignin, were found to have significantly modified solvation under THF-water co-solvent conditions compared to pure water and these modifications were largely independent of temperatures and phase-behaviour. In THF-water, cellulose induces a local phase separation of the co-solvent on its surfaces, with THF primarily located at the hydrophobic faces of cellulose and water on the hydrophilic faces[19, 21]. This phase separation was found experimentally to promote the acid-catalysed hydrolysis of cellulose, allowing for (under optimal conditions) the complete dissolution of cellulose and solubilization of biomass[19].

Missing from these prior studies of biomass in CELF-like conditions has been a detailed examination of the other abundant cell-wall polysaccharide: hemicellulose. Hemicellulose polymers, such as xylan, are more acid labile than glucan cellulose chains, and thus the kinetic rates of cellulose hydrolysis are considerably slower than those of and hemicellulose[22]. This

often necessitates separate processing of each fraction to achieve higher total yields of sugars or sugar-derived products from biomass, a requirement that considerably increases processing costs. THF-water co-solvent, however, has recently been shown to overcome this practical barrier by enabling integrated processing of biomass, such as the high yield co-production of furfural and 5-hydroxymethylfurfural (HMF) from biomass xylan and glucan, respectively[6].

To gain a more complete molecular picture of the CELF pretreatment of biomass, here we combine extensive molecular dynamics (MD) simulations, experimental solubilization studies, dehydration reactions, and reaction kinetics modelling to examine xylan (as a hemicellulose analogue) in CELF-like conditions (THF-water co-solvent). The simulations predict that, unlike lignin polymers and cellulose fibres, xylan solvation in THF-water exhibits a temperature/co-solvent phase dependence. This suggested that, due to the substantial increase of water within of the local solvation of xylan within the miscibility gap, the solubilization of xylan within the miscibility gap temperature regime should be similar to its solubilization in a purely aqueous environment (at the same temperature). Further, as THF will compete for access to xylan outside of the gap we hypothesize that xylan solubilization would be reduced compared to aqueous conditions at temperatures above the biphasic gap. We go on to experimentally validate the above prediction. Additionally, we find that although xylan solubilization is reduced outside of the miscibility gap, xylose dehydration is enhanced. From the combination of these effects and our prior work regarding the enhancement of cellulose hydrolysis in THF-water[19], we posit that these competing effects allow for the 'tunable' products resulting from modified CELF pretreatments. Indeed, we suggest that by selectively controlling the deconstruction of the xylan or glucan components of biomass it is possible, in a single-pot, to effectively co-produce furfural and HMF.

Methods

Molecular Dynamics Simulations

To elucidate and compare the behaviour of xylan (hemicellulose) in aqueous and THF-water co-solvent environments, a linear xylan chain, with a degree of polymerization equal to 30 (*i.e.,* 30 monomer units), was simulated at five temperatures (303K, 350K, 378K, 400K and 445K) and in pure water and in a 1:1 (vol) THF:water mixture. The xylan model was constructed using the Maestro simulation package from Schrodinger, Inc[23], with an initial turn-like structure (Figure 1). The solute was place in the centre of a periodic box with an edge length 13.6 nm and solvated with the GROMACS 5.1 gmx solvate utility.
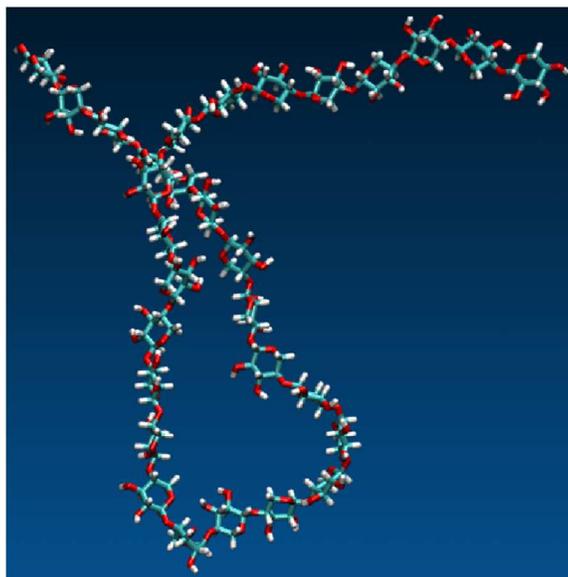
Figure 1. Initial Conformation of xylan.

To improve statistics, five independent simulations were performed at each temperature (303K, 350K, 378K, 400K, and 445K) for a length of 100ns each. All simulations were performed using the GROMACS 5.1 software package[24, 25]. Force-field parameters were obtained from the latest CHARMM force-field[26, 27] using the CHARMM-GUI[28, 29]. Each system

6

was simulated following a typical three-step process: energy minimization, solvent/box relaxation, and production. Energy minimization of the system, with no constraints, was performed for a maximum of 10000 steps for both the co-solvent and pure water systems using the steepest descent algorithm as implemented GROMACS 5.1. Five isobaric-isothermal (NPT) solvent/box relaxation simulations (with the solute constrained in place) at each temperature (303K, 350K, 378K, 400K, and 445K) with a target pressure of 1 Bar were performed using a 0.5fs timestep along with the Berendsen barostat and thermostat[30] with starting configurations taken from the post-energy minimized systems. The solvent/box relaxation simulations were performed for a length of 2.5ns for the xylose-co-solvent system and 1 ns for the water-xylose control system. The short relaxation was performed for this short time to allow a minor expansion of simulation box to avoid unphysical high-pressures and possible initial configuration clashes that may have resulted from the initial model construction.

Following relaxation, production simulations were performed in the NVT ensemble with frames saved every 20ps) and temperatures fixed with the V-rescale thermostat[31]. To allow the use of a 2fs integration step-size for the production simulations, bond lengths were constrained using the LINCS algorithm[32, 33]. For all simulations, long-range electrostatics were treated using the Particle Mesh-Ewald (PME) method as implemented in GROMACS[34]. Analysis was performed using only the last 50ns to avoid any relaxation artefacts.

Computational Analysis

Quantification of the influence of the co-solvent system on the conformational behaviour of xylan was performed by calculating the mass fractal dimension scaling factor (η), shape anisotropy (κ), and chain xylose-xylose (xylan monomer-monomer) radial distribution functions.

The mass fractal dimension scaling factor, η, was obtained by fitting the power-law $R_g = A(n)^\eta$, where R_g is the radius of gyration and n is the number of monomers in the chain, where values of η range from 0 to 1, with values of η greater than 0.5 corresponding to random coil polymer conformation and η less than 0.33 corresponding to collapsed (globule) polymer conformations. Furthermore, the fractal dimension (the reciprocal of η) is directly relatable to the solvent 'quality', with 1/η equal to 2 corresponding to a θ solvent, and when 1/η is approximately equal to 5/3 (for a chain embedded in a 3 dimensional space, and 4/3 when embedded in a 2 dimensional space) the polymer is considered in to be in a 'good' solvent[35].

Shape anisotropy was obtained through the standard relation: $\kappa = \frac{3}{2} \frac{\lambda_x^4 + \lambda_y^4 + \lambda_z^4}{(\lambda_x^2 + \lambda_y^2 + \lambda_z^2)^2} - \frac{1}{2}$, where λ_i are the eigenvalues of the radius of gyration tensor, and κ ranges from 0 to 1, with 0 corresponding to a shape with spherical symmetry and 1 corresponding to a straight line. The eigenvalues necessary to compute the shape anisotropy were calculated using the reduced (all atoms are taken to have a mass of 1) inertia tensor of the xylan molecule (obtained with the built-in VMD[36] measure command) and transformed into the radius of gyration tensor eigenvalues through the relations noted in Suter and Theodorou[37].

Solvent-xylan interactions were quantified by calculating solvent-xylan hydrogen-bonds (with a distance cut-off of 0.3nm and an angle cut-off of 20°) distributions, xylan-water radial distribution functions, and xylan-THF radial distribution functions. To quantify the similarity and difference between the hydrogen-bond distributions, the statistical energy distance measure was used. The statistical energy distance is taken as the integral of the squared difference of the cumulative distribution functions of the distributions, *i.e.,* $D = \int_{-\infty}^{\infty} (F(x) - G(x))^2 dx$, where F(x) and G(x) are the cumulative distribution functions of two different probability distributions[38].

Xylan Solubilization Reactions

Beechwood xylan (BWX, Sigma Aldrich) was used as a model xylan-rich substrate for solubility experiments in water or co-solvent solution. The co-solvent solution was prepared by 1:1 volume addition of THF and water. Before each reaction, 0.3g of BWX was loaded into 12 mL (10mL working volume) T317 stainless steel high pressure "pill" reactors made from standard Swagelok components. 7.7g of water or co-solvent solution was then added to the reactor. For each reaction, the pill reactors were sealed (preventing co-solvent boiling/evaporation) and placed into a metal basket that was submerged into a preheated 4 kW fluidized sand bath (Princeton Techne). Reactors were allowed to preheat for 90 secs in the sand bath before timing of the reaction was started. The reaction was terminated by submerging the pill reactors in a 10-gal room temperature water bath. It should be noted the reactions were performed in triplicate to provide stronger statistical evidence. As lower-molecular weight (MW) xylan solubilizes more readily in pure water than in the co-solvent solution, following termination of the reaction, the product slurry from the water reactions was supplemented with additional pure THF to exactly 1:1 volume ratio, causing additional precipitation of solubilized xylan. The resulting turbid xylan slurry from both water and co-solvent reactions were centrifuged at 15,000 rpms for 15 mins. The now clear contents were dried for 4 hours at 60°C and then 8 hours at 105°C and remaining solids were weighed. This method for determining the solubility has the benefit that even in cases where BWX samples maybe impure the relative differences between the solvent conditions will still be made clear[39].

Xylose and Maple Wood Reactions

For xylose and maple wood reactions, 10 g of D-xylose (>99% purity, Sigma-Aldrich, St. Louis, MO) or 40g maple wood was transferred to a 1 L volumetric flask and dissolved with either water-only or 1:1 THF:water co-solvent solution containing 0.1M sulfuric acid concentration. It should be noted that the mechanically stirred Hastelloy® Parr (Parr Instrument Company, Moline IL) reactors, rather than unstirred 'pill' reactors, were necessary for reacting maple wood to allow the use of the 0.1M H_2SO_4 and to avoid mass-transfer limitations. The combined contents were then poured into a 1 L Hastelloy® Parr stirred reactor with twin pitched 6 blade impellers and sealed. The Parr reactor was then submerged into the 1 kW fluidized sand bath preheated at twice the intended reaction temperature. Heat-up time is typically 3-4 mins and reaction time is started when reactor temperature reaches within 1K of intended reaction temperature. Heating was controlled by adjusting the height of the reactor over the sand bath after initial heat-up to ensure that the target temperatures were not "overshot." To terminate reactions, the entire reactor is transferred and submerged into a 10-gal room temperature water bath. The solid contents are separated by vacuum filtration through a paper filter (Fisher Scientific, Waltham MA), and the liquids are diluted in water and analysed by HPLC equipped with an Aminex® HPX-87H column (Bio-rad, Irvine, CA). For calculation of rate constants, a first-order approximation of xylose dehydration is represented by Equation (1)

(1) $Xylose \xrightarrow{k_1} D$

where D represents degradation products. The expression for the rate of xylose (X) disappearance and calculation of the rate constant are given in Equations (2), (3), and (4). Since acid concentration (A) was held constant throughout our studies, it was combined into the overall rate constant k.

(2) $\frac{d(X)}{dt} = -(k_1 A)X = -kX$ (k = lumped acid term)

(3)
$$\int_{X_{init.}}^{X} \frac{d(X)}{X} = -k \int_0^t dT$$

(4)
$$\ln\left(\frac{X}{X_{init.}}\right) = -kt$$

where rate constant k was determined by linear fitting of Equation (4). Results after 30 min were not used in the linear fitting as the xylose solution became too dilute for accurate quantification.

Results.

We first present our computational work (Figures 2 through 8 and Table 1) followed by our experimental work (Figures 9 and 10).

Xylan Conformational Behaviour
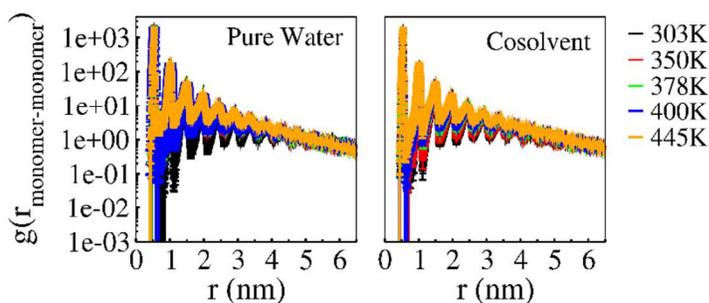
Figure 2. Average Xylose-Xylose Radial Distribution Functions. Colours indicate different temperatures, and error-bars are less than or equal to the width of the

The xylan monomer-monomer (xylose-xylose) radial distribution function provides a direct measure for the ordering of the monomers of the polymer. Figure 2 indicates that this ordering is long-ranged: distinct peaks, a signature of order, are found even at distances greater than 4nm for temperatures less than 400K and near ≈ 3nm at 445K (see figure SI-I-V for images of each temperature separately). Another important finding is that the profiles are nearly indistinguishable when comparing either between temperatures or solvent conditions.

Distributions of the mass fractal dimension scaling constant and the shape anisotropy are shown in Figures 3 and 4; the distributions again show only minor differences between water-only and THF-water environments at T>303K, with strong overlapping of the peak locations for the distributions. Focusing first on the fractal dimension scaling constant distributions, the
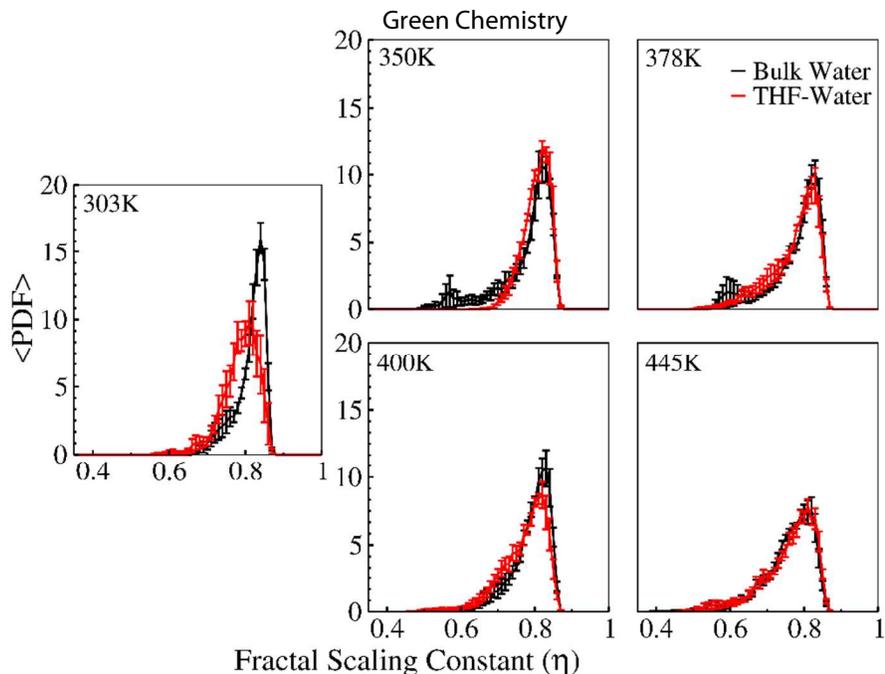
Figure 3. Average Distributions of Fractal Scaling Constants. Colour indicates the solvent type. Error-bars are standard error of the mean.

average scaling constant is between 0.76 and 0.81. This corresponds to 'good' solvent conditions

for both bulk water and TH-water co-solvent, with mass fractal dimensions (the reciprocal of η)

ranging from 1.25 to 1.32[35].

The shape of the xylan chain was probed by calculating its shape anisotropy (Figure 4).
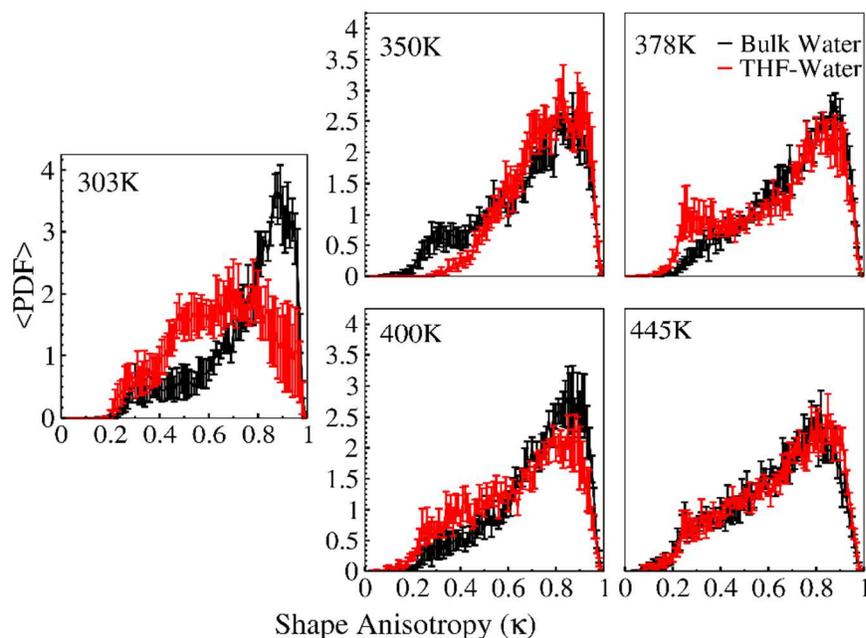
Figure 4. Average Shape Anisotropy Distributions. Colour indicates solvent condition. Error-bars are standard error of the mean

Under all temperatures, the distributions have peaks well above 0.5 (corresponding to anisotropic

structures). Indeed, at T>303K, the peaks are >0.8 for all solvent conditions, nearing the linear

regime whose anisotropy is 1. Similar to Figures 2 and 3, at T>303K, the peaks of the

distributions are strongly overlapping. Taking all the xylan conformational metrics into account

(Figures 2-4), we conclude that xylan conformations are similar in THF-water and pure water.

Furthermore, these structural measures suggest that both solvent conditions are 'good' solvents.

Xylan-Solvent Interactions

Xylan solvation is characterized here by two measures: solvent-xylan hydrogen bonding and

radial distribution functions of the solvent components about the xylan chain. Figure 5 shows

that independent of temperature, both the average and maximum number of HBs between the
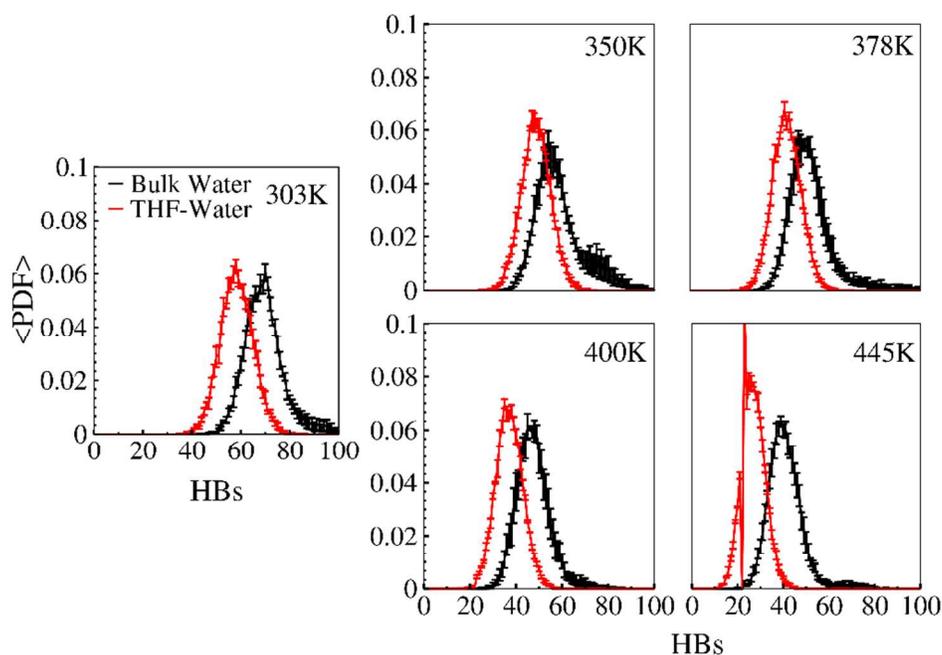
Figure 5. Average distributions of the number of (co)solvent-xylose hydrogen bonds. Error bars are of the standard error of the mean.

solvent and xylan are decreased in the co-solvent when
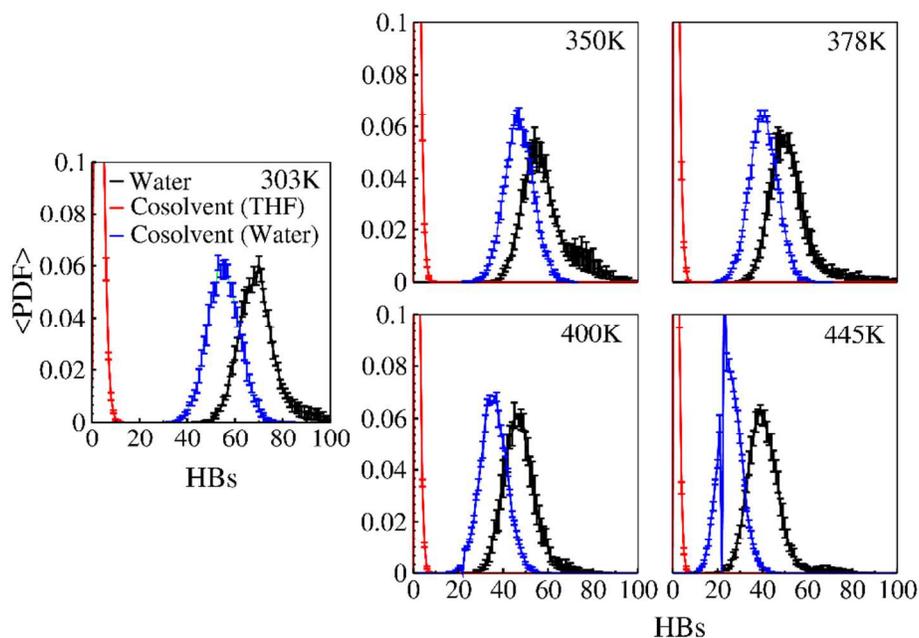
Figure 6. Average decomposed co-solvent-xylose hydrogen-bond number distributions. Error-bars are the standard error of the mean.

$$D = \int_{-\infty}^{\infty} [(CDF(X)_{\text{Xylan-Solvent HBs}}) - (CDF(x)_{\text{Xylan-Cosolvent HBs}})]^2 dx$$
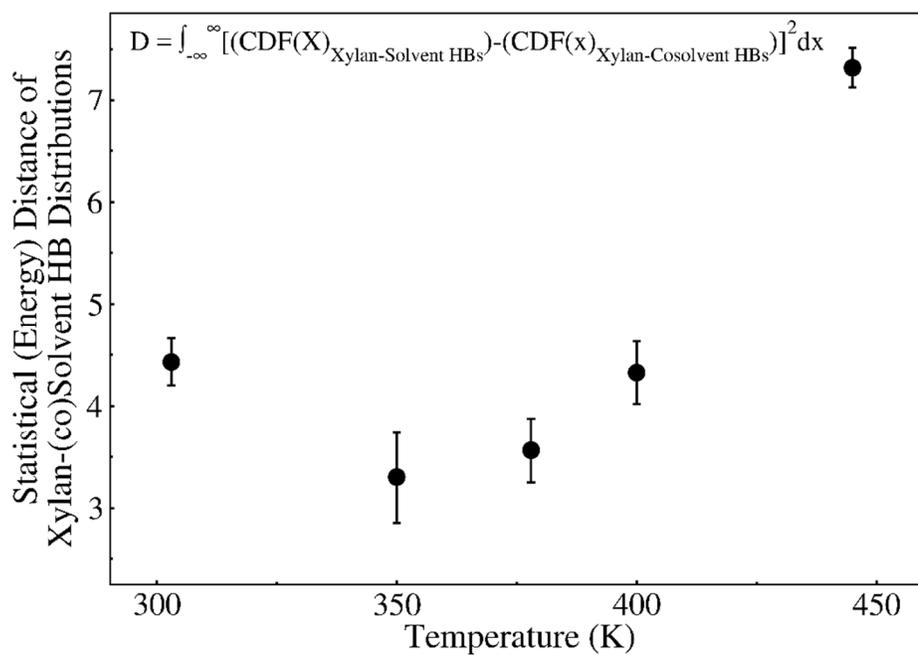
Figure 7. Average statistical (energy) distance between solvent and co-solvent distributions. Error bars are standard error of the mean.

compared to pure water. Interestingly, as the temperature enters the miscibility-gap (demixing)

regime (350K-400K), the distributions appear to approach one another.

Decomposing the distributions of co-solvent-xylan HBs into THF-xylan and water-xylan HBs (figure 6), shows that it is the water-xylan HBs that are most affected by temperature. Figure 7 provides the statistical energy distance[38] between the distributions in Figure 5, which quantifies the "distance" between these distributions and makes clear that indeed they approach one another in the miscibility gap. Additionally, the energy distance reaches a maximum (for the temperatures used in this study) at T=445K, above the miscibility gap.

Continuing the examination of the (co)solvent-xylan interactions, Figure 8 shows the solvent/co-solvent component-xylan radial distribution functions. Comparing the water-xylan radial distribution functions between the pure water and co-solvent systems shows that in the co-solvent, water solvation ("hydration") depends on temperature with increased hydration at T=350K to T=400K, while in pure water hydration is independent of temperature. Furthermore,
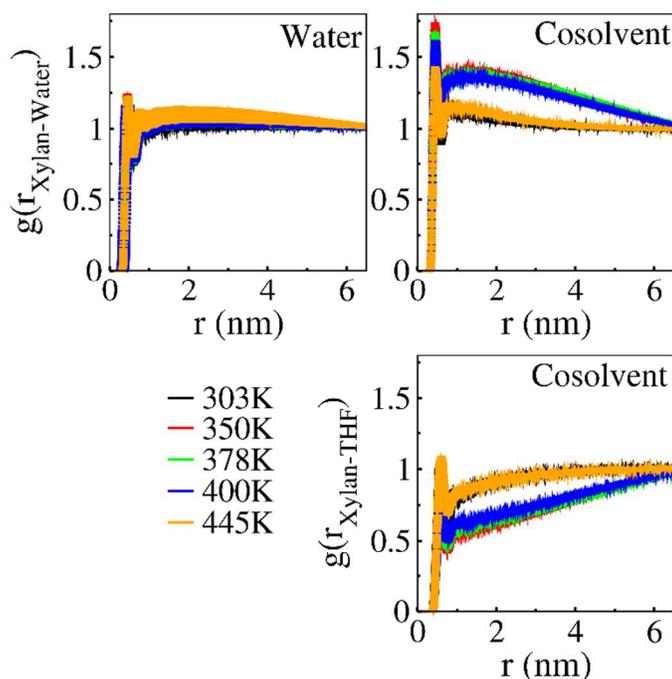
Figure 8) Xylose-Solvent Component Radial Distribution functions. Error bars are of the standard error of the mean and are less than or equal to the width of the line.

16

for the co-solvent system, as water solvation increases between T=350-400K, the presence of THF in the solvation shell is decreased (though the local solvation shell does not entirely exclude THF). This indicates that within the miscibility gap the local solvent near xylan is primarily water with THF (largely) displaced.

The computational measures (Figures 1-8) indicate that, although xylan adopts conformations consistent with a polymer in a"good" solvent at all temperatures, xylan solvation depends on temperature: above and below the THF-water miscibility gap, xylan's local solvent is composed of both water and THF, whereas it is mostly water within the gap. Given the preferential water solvation within the gap, we hypothesize that xylan solubilization within the miscibility gap would be similar to xylan solubilization in purely aqueous conditions. Further, we hypothesize that as THF displaces water from the xylan solvation shell at temperatures above the miscibility gap, xylan solubilization will be reduced compared to pure water conditions. To validate these predictions, we performed a comparative experimental solubilization study of beechwood xylan in both water and THF-water within and outside of the miscibility gap temperature regime. This was complimented with dehydration kinetics of xylose in both water and THF-water.

Temperature-dependent phase behaviour reduces solubilization of xylan in co-solvent
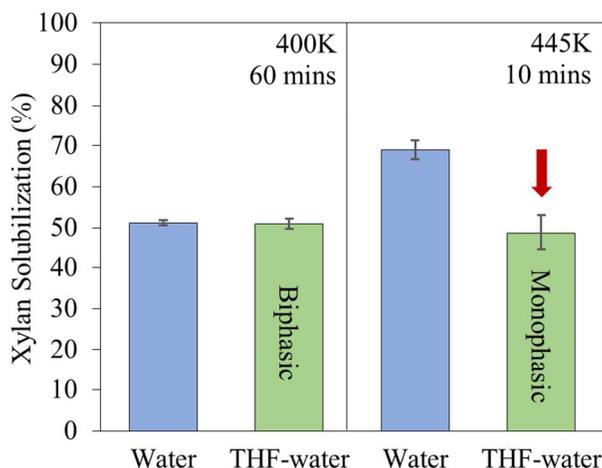
Figure 9. Solubilization of beechwood xylan (BWX) after treatment in water and 1:1 THF:water co-solvent environment at 400K and 445K. The reaction time is reduced at 445K to more closely resemble 400K data in order to show depression of xylan solubilisation in monophasic THF-water.

In order to evaluate the effect of the temperature-dependent phase behaviour of THF and water on xylan solubilization, beechwood xylan (BWX) was treated under autoclave pressures in both 1:1 (vol) THF:water and in pure water at two temperature-phase conditions: 400K, at which THF-water is biphasic and 445K, where THF-water is monophasic. Because increasing the reaction temperature increases the rate of xylan solubilization, independent of phase behaviour, the treatment time in this experiment was reduced from 60 mins at 400K to 10 mins at 445K. This led to the total xylan solubilized in the different THF:water phase regimes being approximately matched, thus better illustrating the phase-dependent effects, rather than temperature-dependent effects, as shown in Figure 9. The difference in total solid mass of BWX before and after treatment (as described in the Methods section) was used to determine xylan solubilization, which is influenced both by changes to local solvation (which were quantified in the simulations by the solvent-xylan radial distribution functions) and depolymerization by hydrolysis. We observed that at 400K, the extent of BWX solubilization is similar between pure water and THF-water, with about 50% of total solids solubilized in both cases. As anticipated by

the local solvation calculated in our simulations and a previous study[40], the rate of reaction of water-soluble xylan components in a biphasic system is similar to an aqueous-only system and BWX solubilization is independent of the presence (or absence) of THF. However, at 445K THF and water are miscible, and the presence of THF in the co-solvent is shown to have significantly decreased xylan solubilization by 40% when compared to the water-only case absent of THF (Figure 9). The solubilization of BWX in THF-water at 445K and 10 mins was nearly identical to that achieved at 400K and 60 min, indicating a 2-fold decrease in solubilization rate approximated from the pretreatment severity factor (rate doubles every increase of 10K).

Reduced xylan solubilization and increased xylose dehydration in monophasic THF-water improves one-pot production of furfurals from biomass

The production of furfurals, such as furfural and 5-HMF, from lignocellulosic biomass has recently drawn significant scientific interest due to their suitability as green platform molecules for subsequent conversion to transportation fuels and renewable chemicals[41]. Furfural and 5-HMF are the catalytic dehydration products of xylose and glucose, respectively, which are the catalytic or enzymatic hydrolysis products of xylan and glucan in lignocellulosic biomass, respectively. As they are both derived from biomass, efforts to understand how to improve their co-production is a crucial strategy for reducing the cost of future biofuels. To examine how depression of xylan solubilization in monophasic THF co-solvent environment can influence the production of furfural and 5-HMF from biomass, we must first independently evaluate the influence of THF-water on the following sequence of events: 1) xylan and glucan are first solvated before 2) undergoing depolymerization to xylose and glucose by acid-catalysed hydrolysis, then 3) xylose and glucose further undergo dehydratation chemical reactions to furfurals under acidic conditions.

Thus, to determine the rate of xylose (the monomer of xylan) conversion to furfural by acid-catalysed dehydration, we heated xylose solutions to 445K in both water and THF co-solvent mixtures and tracked xylose disappearance and its subsequent selective transformation to furfural over time, as shown in Figure 10A. For these reactions, 0.1M dilute sulfuric acid was added to both solvent environments as a catalyst and at concentrations conducive to achieving high furfural yields from biomass[41]. Using first order kinetics, the rate of xylose disappearance was found to be two-fold higher in the monophasic THF co-solvent environment as compared to only water (Figure 10A and Table S1 in the Supplementary). Thus, our study finds that THF-water in the monophasic regime can accelerate the disappearance rate of xylose while delaying the formation of furfural. Supporting evidence suggests that the longer open-chain pathway via isomerization to xylulose[42] is dominant here instead of the shorter closed-chain pathway via ring contraction[43] that is dominant in pure water. As such, the maximum selectivity of furfural occurred at 10 mins in the water-only reactions, much earlier than in the miscible THF-water reactions, where maximum furfural selectivity was achieved later at 40 mins. It is worth noting (see Discussion) that cellulose solubilization is enhanced and 5-HMF production accelerated in miscible THF-water under the same acidic conditions.
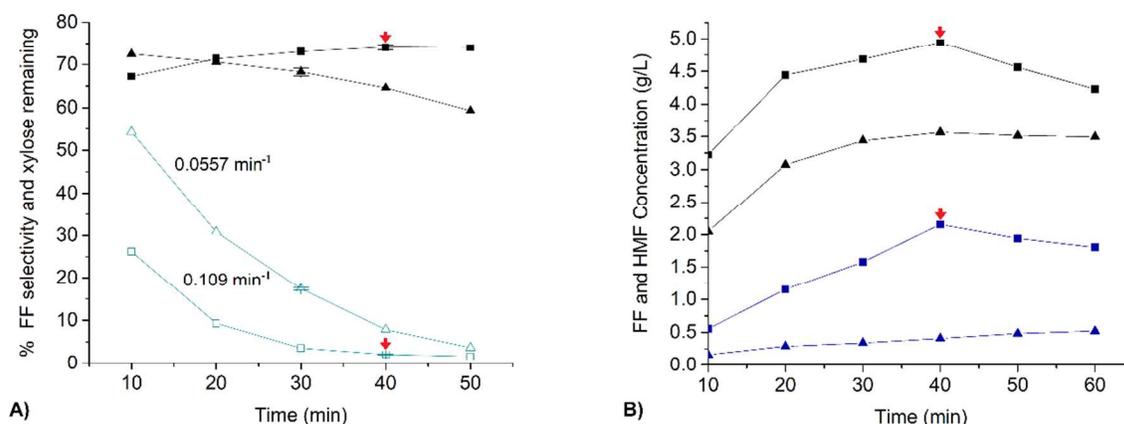
Figure 10. A) Furfural (FF) selectivity and xylose disappearance from dilute sulfuric acid reactions of xylose in water (▲) and in THF-water co-solvent (■). B) Concentration of FF (black) and 5-HMF (blue) from dilute sulfuric acid reactions of maple wood chips in water (▲) and in THF-water co-solvent (■). Red arrows were drawn at optimal or maximum values for each species.

To translate our findings to understanding the conversion of C5 and C6 components in whole biomass to furfural (from xylan) and 5-HMF (from cellulose), we performed comparative reactions starting from raw maple wood chips at the same temperature (445K) as the xylan reactions and tracked the resulting liquid concentrations of furfural and 5-HMF over time, as shown in Figure 10B. Interestingly, due to the slower solubilization of xylan and delayed formation of furfural from xylose in monophasic THF-water, the concentration of furfural steadily increased for 40 mins of reaction before declining. In the water-only case, however, more rapid solubilisation of xylan to xylose followed by more rapid formation of furfural resulted in achieving near maximum furfural yield much sooner as well as a notable 40% lower maximum yield. Similarly, for the cellulose pathway, a very prominent maximum in 5-HMF concentration was observed also at 40 mins in the co-solvent reactions, whereas very little 5-HMF was observed from maple wood in the water case, slowly increasing in concentration over time with no clear maximum within 60 mins. This is due to the very slow release of glucose from cellulose in water-only followed by rapid degradation of 5-HMF to levulinic acid and formic acid.

Discussion

From our computational characterization of xylan structure and solvation (Figures 2-8), it was shown that for both pure water and THF-water co-solvents both solvents act as 'good' solvents for xylan. This contrasts with lignin, which is compact in pure water (aqueous solutions)

but becomes extended and more accessible to the solvent in THF-water co-solvents at temperatures greater than 283K[18-21].

The similarity of the xylan conformations in both aqueous and co-solvent environments is not entirely surprising as it is well known that both bulk THF and water can serve as 'good' solvents for xylose. Indeed, THF solutions, with an acid catalyst, can readily convert xylose to furfural[44]. What is surprising is that, unlike previous investigations of cellulose and lignin in THF-water co-solvents, where make-up of the solvation shells of the polymers was found to have negligible temperature dependence, the make-up of the solvation shell of xylan is temperature dependent and related to the co-solvent phase behavior[19, 45, 46]. Indeed, xylan experiences a significant reduction of THF (and an associated increase in water) within its solvation shell when temperatures are within THF-water miscibility gap (biphasic regime). This modification in solvation structure suggested that within this gap, xylan solubilization should be similar to that found in purely aqueous environments. Further, from the model we hypothesized that at temperatures above of the gap (monophasic regime), xylan solubilization would be reduced relative to purely aqueous conditions.

Our comparative solubilization experiments on BWX validated the computational predictions of dramatically reduced xylan solubilization in miscible THF-water. We also observed that although the rate of disappearance of xylose monomers in miscible THF-water was faster than that of bulk water, the formation of furfural was slower. These seemingly contradictory results are in fact compatible when considering that the MD calculations investigated the solvationof xylan polymres rather than xylose. Chemical reactions then dominated the subsequent steps of xylose isomerization followed by acid-catalyzed dehydration. As such, the delay of both xylan solubilization and of maximum furfural production under

miscible THF-water conditions is an important outcome for supporting the co-production of furfural and 5-HMF from biomass.

Furfural is highly reactive and degrades quickly in the presence of dilute acid at elevated temperatures, thus milder reaction conditions are generally favored in order to reduce the rate of furfural degradation in order to achieve sufficiently high yields from biomass[47]. Conversely, the production of 5-HMF from glucan in cellulose is much slower due to the slower rate of hydrolysis of glucan in pure water, thus requiring more severe reaction conditions to accelerate 5-HMF production. During reaction of whole biomass, these two competing factors are combined, and furfural losses usually greatly exceed the rate of 5-HMF production, creating a highly undesirable situation. Overcoming this kinetic disparity in hydrolysis and dehydration events between the C5 and C6 pathways typically require a two-stage reaction scheme so that furfural can first be independently targeted with a milder temperature reaction followed by a hotter 5-HMF reaction and/or require the use of an immiscible extracting solvent to reduce furfural and 5-HMF losses[40, 48, 49].

Unlike these costly two-stage methods, unique synergies can be observed in the monophasic THF co-solvent system allowing integrated processing of biomass to achieve greater process efficiencies and yields. As shown here, delayed furfural formation resulting from slower xylan solubilization in monophasic THF-water reaction improves the kinetics for the C5 pathway. We also recently discovered an opposite effect for the C6 pathway, where we reported that treating cellulose or biomass in miscible THF-water at 445K dramatically improved its solubilization to glucose due to local partitioning of THF and water along the cellulose fiber[19]. As a result, the delayed production of furfural from slower xylan solubilization and the improved production of 5-HMF from increased cellulose solubilization in monophasic THF-water enables

the pairing of optimal reaction conditions that explain how high yield co-production of furfural and 5-HMF directly from biomass can be achieved by a single integrated reaction[6].

Conclusion

The miscibility of THF-water changes at distinct temperature ranges. Our combined computational and experimental work has demonstrated that, unlike the solvation of lignin and cellulose, xylan (hemicellulose) solvation, and consequently, solubilization, are phase-dependent in a THF-water system, with water becoming the dominant component of the xylan solvation shell within the miscibility gap (biphasic). We further demonstrated through experimental THF-water reactions of xylose and maple wood at miscible conditions (445K), that the reaction time to achieve maximum furfural yields is longer whereas the time to achieve maximum 5-HMF yields is shorter, both occurring favorably at 40 mins of reaction time. The combination of these effects reveals that the mechanism permitting high yields co-production of HMF and furfural from biomass is that the slower hydrolysis of glucan (in cellulose) is able to "catch-up" with the faster hydrolysis of xylan.

Acknowledgements

resources of the Compute and Data Environment for Science (CADES) at the Oak Ridge National Laboratory, which is supported by the Office of Science of the U.S. Department of Energy under Contract No. DE-AC05-00OR22725 and the resources of the National Energy Research Scientific Computing Center, a DOE Office of Science User Facility supported by the Office of Science of the U.S. Department of Energy under Contract No. DE-AC02-05CH11231.

References

1.　S. Singh, G. Cheng, N. Sathitsuksanoh, D. Wu, P. Varanasi, A. George, V. Balan, X. Gao, R. Kumar and B. E. Dale, *Frontiers in Energy Research*, 2015, **2**, 62.
2.　S. P. Chundawat, B. S. Donohoe, L. da Costa Sousa, T. Elder, U. P. Agarwal, F. Lu, J. Ralph, M. E. Himmel, V. Balan and B. E. Dale, *Energ Environ Sci*, 2011, **4**, 973-984.
3.　H. L. Trajano, N. L. Engle, M. Foston, A. J. Ragauskas, T. J. Tschaplinski and C. E. Wyman, *Biotechnol Biofuels*, 2013, **6**, 110.
4.　T. Y. Nguyen, C. M. Cai, R. Kumar and C. E. Wyman, *ChemSusChem*, 2015, **8**, 1716-1725.
5.　C. M. Cai, T. Zhang, R. Kumar and C. E. Wyman, *GREEN CHEMISTRY*, 2013, **15**, 3140-3145.
6.　C. M. Cai, N. Nagane, R. Kumar and C. E. Wyman, *GREEN CHEMISTRY*, 2014, **16**, 3819-3829.
7.　J. Matous, J. Sobr, J. Pick and J. P. Novak, *Collection of Czechoslovak Chemical Communications*, 1972, **37**, 2653-&.
8.　A. Oleinikova, I. Brovchenko, A. Geiger and B. Guillot, *J Chem Phys*, 2002, **117**, 3296-3304.
9.　O. Kiyohara and G. C. Benson, *Canadian Journal of Chemistry-Revue Canadienne De Chimie*, 1977, **55**, 1354-1359.
10.　D. Zikmundova, J. Matous, J. P. Novak, V. Kubicek and J. Pick, *Fluid Phase Equilibr*, 1990, **54**, 93-110.
11.　M. D. Smith, B. Mostofian, L. Petridis, X. Cheng and J. C. Smith, *J Phys Chem B*, 2016, **120**, 740-747.
12.　I. Brovehenko and B. Guillot, *Fluid Phase Equilibr*, 2001, **183**, 311-319.
13.　D. T. Bowron, J. L. Finney and A. K. Soper, *J Phys Chem B*, 2006, **110**, 20235-20245.
14.　A. C. Kumbharkhane, S. N. Helambe, M. P. Lokhande, S. Doraiswamy and S. C. Mehrotra, *Pramana-Journal of Physics*, 1996, **46**, 91-98.
15.　D. T. Bowron, J. L. Finney and A. K. Soper, *J Am Chem Soc*, 2006, **128**, 5119-5126.
16.　Y. Sun and J. Y. Cheng, *Bioresource Technol*, 2002, **83**, 1-11.
17.　R. Kaida, T. Kaku, K. i. Baba, M. Oyadomari, T. Watanabe, K. Nishida, T. Kanaya, Z. Shani, O. Shoseyov and T. Hayashi, *Molecular Plant*, 2009, **2**, 904-909.
18.　M. D. Smith, B. Mostofian, X. L. Cheng, L. Petridis, C. M. Cai, C. E. Wyman and J. C. Smith, *Green Chem*, 2016, **18**, 1268-1277.

19. B. Mostofian, C. M. Cai, M. D. Smith, L. Petridis, X. L. Cheng, C. E. Wyman and J. C. Smith, *J Am Chem Soc*, 2016, **138**, 10869-10878.
20. M. D. Smith, L. Petridis, X. L. Cheng, B. Mostofian and J. C. Smith, *Phys Chem Chem Phys*, 2016, **18**, 6394-6398.
21. M. D. Smith, X. L. Cheng, L. Petridis, B. Mostofian and J. C. Smith, *Sci Rep-Uk*, 2017, **7**.
22. P. Kanchanalai, G. Temani, Y. Kawajiri and M. J. Realff, *Reaction Kinetics of Concentrated-Acid Hydrolysis for Cellulose and Hemicellulose and Effect of Crystallinity*, 2016.
23. *Journal*, 2015.
24. M. J. Abraham, T. Murtola, R. Schulz, S. Páll, J. C. Smith, B. Hess and E. Lindahl, *SoftwareX*, 2015, **1–2**, 19-25.
25. S. Pall, M. J. Abraham, C. Kutzner, B. Hess and E. Lindahl, *Lect Notes Comput Sc*, 2015, **8759**, 3-27.
26. O. Guvench, S. N. Greene, G. Kamath, J. W. Brady, R. M. Venable, R. W. Pastor and A. D. Mackerell, *J. Comput. Chem.*, 2008, **29**, 2543-2564.
27. O. Guvench, E. Hatcher, R. M. Venable, R. W. Pastor and A. D. MacKerell, *J. Chem. Theory Comput.*, 2009, **5**, 2353-2370.
28. J. Lee, X. Cheng, J. M. Swails, M. S. Yeom, P. K. Eastman, J. A. Lemkul, S. Wei, J. Buckner, J. C. Jeong, Y. F. Qi, S. Jo, V. S. Pande, D. A. Case, C. L. Brooks, A. D. MacKerell, J. B. Klauda and W. Im, *J Chem Theory Comput*, 2016, **12**, 405-413.
29. S. Jo, T. Kim, V. G. Iyer and W. Im, *J Comput Chem*, 2008, **29**, 1859-1865.
30. H. J. C. Berendsen, J. P. M. Postma, W. F. Vangunsteren, A. Dinola and J. R. Haak, *J Chem Phys*, 1984, **81**, 3684-3690.
31. G. Bussi, D. Donadio and M. Parrinello, *J Chem Phys*, 2007, **126**.
32. B. Hess, H. Bekker, H. J. C. Berendsen and J. G. E. M. Fraaije, *J Comput Chem*, 1997, **18**, 1463-1472.
33. B. Hess, *J Chem Theory Comput*, 2008, **4**, 116-122.
34. M. J. Abraham and J. E. Gready, *J Comput Chem*, 2011, **32**, 2031-2040.
35. M. Daoud, H. E. Stanley and D. Stauffer, in *Physical Properties of Polymers Handbook*, ed. J. E. Mark, Springer New York, New York, NY, 2007, DOI: 10.1007/978-0-387-69002-5_6, pp. 83-89.
36. W. Humphrey, A. Dalke and K. Schulten, *J Mol Graph Model*, 1996, **14**, 33-38.
37. D. N. Theodorou and U. W. Suter, *Macromolecules*, 1985, **18**, 1206-1214.
38. M. L. Rizzo and G. J. Szekely, *Wires Comput Stat*, 2016, **8**, 27-38.
39. S. R. Wang, B. Ru, H. Z. Lin and Z. Y. Luo, *Bioresource Technol*, 2013, **143**, 378-383.
40. R. Weingarten, J. Cho, J. W. C. Conner and G. W. Huber, *Green Chem*, 2010, **12**, 1423-1429.
41. C. M. Cai, T. Zhang, R. Kumar and C. E. Wyman, *Journal of Chemical Technology & Biotechnology*, 2014, **89**, 2-10.
42. B. Danon, G. Marcotullio and W. de Jong, *Green Chem*, 2014, **16**, 39-54.
43. M. R. Nimlos, X. Qian, M. Davis, M. E. Himmel and D. K. Johnson, *The Journal of Physical Chemistry A*, 2006, **110**, 11824-11838.
44. X. Hu, R. J. M. Westerhof, D. H. Dong, L. P. Wu and C. Z. Li, *Acs Sustain Chem Eng*, 2014, **2**, 2562-2575.

45.　　M. D. Smith, B. Mostofian, X. Cheng, L. Petridis, C. M. Cai, C. E. Wyman and J. C. Smith, *Green Chem*, 2016, **18**, 1268-1277.
46.　　M. D. Smith, L. Petridis, X. Cheng, B. Mostofian and J. C. Smith, *Phys Chem Chem Phys*, 2016, **18**.
47.　　B. Danon, L. Van der Aa and W. De Jong, *Carbohydrate research*, 2013, **375**, 145-152.
48.　　B. Saha and M. M. Abu-Omar, *Green Chem*, 2014, **16**, 24-38.
49.　　S. Dutta, S. De, B. Saha and M. I. Alam, *Catal. Sci. Technol.*, 2012, **2**, 2025-2036.

Supplementary Information

Table S1. First-order rate constants for the disappearance of xylose in water and THF co-solvent environments

Rate Constant	1:1 THF:water (A/min)	Water (A/min)	Literature (A/min)
k^b	0.109 ± 0.015	0.0557 ± 0.0018	0.0527^c

[a] Reaction conditions: 10 g L^{-1} D-xylose and 1 wt% H_2SO_4 in batch reactions at 170 °C. THF co-solvent solution contained 1:1 THF and DI water. [b] Rate constant includes a 0.204 M hydrogen ion (A) term. [c] Calculated from equations described by K.J. Zeitsch (2000).

Figures S1-S5. Individual Plots of Xylan monomer-monomer radial distribution functions

28
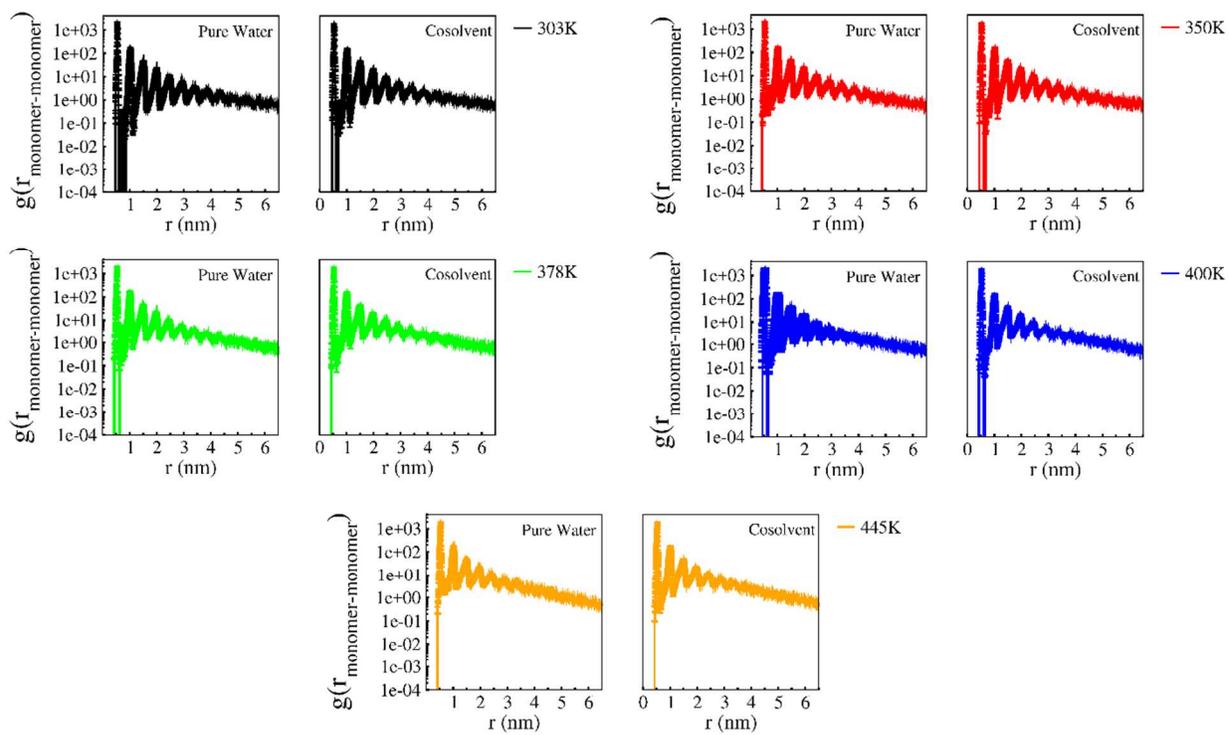
TOC:
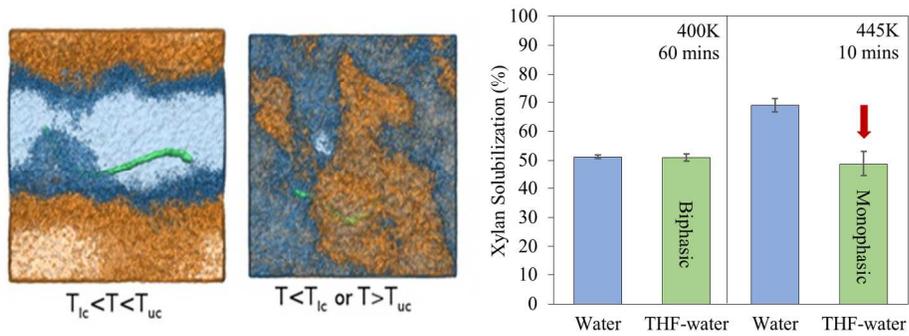
Selective solvation of xylan by water in the THF-Water miscibility gap allows tunable solubilization